

## INCREASED BIOCOMPATIBILITY AND BIOACTIVITY OF SURFACES AFTER ENERGETIC PVD SURFACE TREATMENTS

S. Mändl\*

*Leibniz-Institut für Oberflächenmodifizierung, Leipzig, Germany*

Keywords: Biomaterials, Biocompatibility, Bioactivity, Ion-implantation, Metallic biomaterials, Plasma surface treatments.

### ABSTRACT

*The identification of life and the distinction against inorganic context is nearly as old as mankind. In this paper, energetic coating and implantation processes are briefly introduced, followed by a presentation of the state-of-the-art of surface modification of metals with energetic ions, concentrating on stainless steel, CoCr alloys, titanium alloys, NiTi shape memory alloys and bioresorbable magnesium alloys.*

### 1. INTRODUCTION

The identification of life and the distinction against inorganic context is nearly as old as mankind. Looking at life on Earth, a large assortment of shapes and forms is encountered, which often leads to the assertion that structure alone would allow an identification, e.g. in the case of the Martian meteorite ALH84001 [1]. However, early in the 20<sup>th</sup> century, this rather naïve notion that life has characteristic forms distinguishing it from non-living species was refuted by showing that patterns and forms in nature alone do not allow such a verdict [2,3] – and concurrently influencing the development of Art Nouveau in its due course. Physical causes lead to the formation of honeycombs, similar to hexagonal, basalt rock formation, mineral cages of the radiolarian *Aulonia hexagona* resembling buckminsterfullerenes [4], or nacre formed by mollusks similar to naturally formed agate [5].

However, even advances in genomics and proteomics do not allow a direct explanation of how such structures are formed. Looking more closely at organisms, there are much more compounds than genes and proteins inside them: sugars, lipids, salts and minerals. Consequently, additional forces beside traditional biochemical interactions are acting as guiding principles. Chemical interactions with single atoms, molecules or ions are augmented by purely physical interactions centered on surface energies or electrostatic interactions. Correspondingly, blood coagulation activated by electron transfer reactions [6] or protein production modulated by nanostructured surfaces [7] have been recognized. In turn, different interaction mechanisms are defining the biocompatibility and bioactivity of medical devices. As present day biomaterials, despite tremendous advances obtained within the last 50 years [8,9], revision rates of up to 5 – 15% are nowadays still encountered in clinical applications [10]. These failure causes can be loosely grouped into

four different categories: i) corrosive failure by out-diffusion of metallic cations [11,12]; ii) abrasive wear with particles in the micrometer and nanometer range [13,14]; iii) adverse topography ranging from the atomic to mesoscopic scales [15,16]; iv) non-hydrophilic surface [17].

The worldwide market for metallic biomaterials is predicted to growth with double-digit rates for a least five more years. The major markets are joint reconstruction and trauma fixation, where the volume exceeded \$15 billion in 2008. Organic replacement materials, obtained either from tissue engineering or gene therapy will not be available in the near future as the necessary mechanical stability has presently not been achieved in the laboratory. As surgeons have to employ metallic materials, different strategies are currently used to address the mentioned failure causes. However, each cause is addressed separately and differently.

One breakthrough would be to address the individual origins of failure using one process, e.g. one single surface modification technology with the process parameters adjusted correspondingly. The aim is to provide a specifically tailored surface can be provided with synergistic effects encompassing several interaction mechanisms simultaneously. In this presentation, energetic coating and implantation processes are briefly introduced, followed by a presentation of the state-of-the-art of surface modification of metals with energetic ions, concentrating on stainless steel, CoCr alloys, titanium alloys, NiTi shape memory alloys and bioresorbable magnesium alloys.

### 2. EXPERIMENTAL

The main parameter characterizing energetic surface modifications is the incident particle or ion energy. For low kinetic energies the incoming ion will be stopped within the first monolayer or even at the surface itself if the energy is too low to create atomic displacements inside the target material [18]. Thus, a deposition onto the surface can be observed for energies below 5 – 10 eV. These physical vapor deposition (PVD) processes encompass, with increasing energy per deposited particle: evaporation, reactive sputtering, vacuum arc deposition and ion beam assisted deposition (IBAD) techniques [19-21]. By increasing the average particle energy, a distinct development of the surface morphology is observed, first described by Thornton [22]. As shown in Fig. 1, with increasing bombardment, the films become denser with a reduced void fraction, caused by an enhanced

\* stephan.maendl@iom-leipzig.de

surface mobility and larger crystallites due to Ostwald-ripening of the initially nucleated nanocrystals [23]. At the same time, a higher average energy per deposited particle leads to a reduced surface roughness as the enhanced surface mobility leads to a mass transport on the surface.

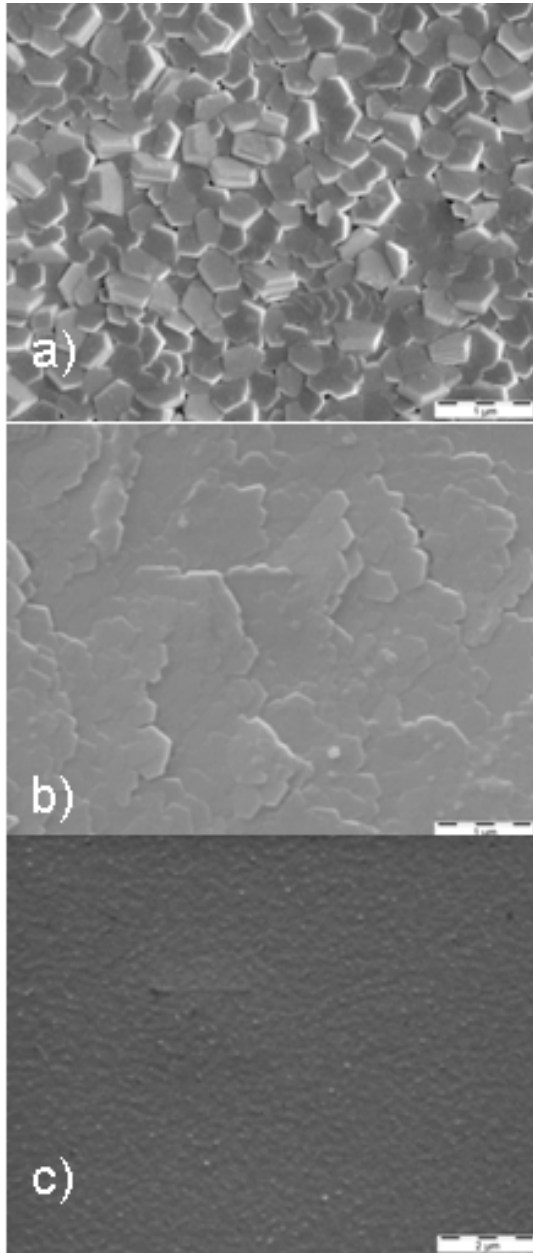


**Figure 1 - Surface morphology of Mg films deposited at room temperature with a rate of about 1  $\mu\text{m}/\text{h}$  by (a) magnetron sputtering, average energy  $\sim 8$  eV, (b) ion beam sputtering, average energy  $\sim 12$  eV, and (c) vacuum arc deposition, average energy  $\sim 25$  eV [26].**

Ion implantation itself was developed in the early 1950s by Shockley in the Bell Laboratories and is nowadays indispensable in the semiconductor industry [24]. Here, a controlled insertion of foreign atoms below the surface is obtained with the ion range, and hence the modification depth, vary-

ing between a few nanometers to several micrometers. Atomically mixed solid solution of the inserted atoms in the host matrix are present for low fluences. With increasing fluence, the coalescence of precipitates into closed layers is occurring. In addition to the possibility of implanting any chemical element into any matrix, ion implantation is characterized by the possible formation of metastable phases far from the thermodynamic equilibrium [25].

However, conventional ion implantation is limited to small and flat substrates as a small beam exiting the beamline has to be scanned across the target. By removing this beamline and inserting the target directly into the plasma source, implantation into arbitrarily shaped objects is possible by applying negative high voltage pulses, a process called plasma immersion ion implantation (PIII) [27,28]. During the pulses, positive ions are extracted from the plasma and accelerated towards the whole surface simultaneously. This method combines the advantages of plasma treatments, like PVD processes or plasma nitriding, and ion implantation in one method.

For fundamental investigations, flat polished coupons were used in the experiments. The materials investigated in different experiments include Ti grade 2 (Ti  $> 99.2\%$ , O  $\leq 0.25\%$ ), Ti grade 5 (Ti6Al4V), SM 495 (54.5% Ni, 45.5% Ti), SE 508 (55.8% Ni, 44.2% Ti), stainless steel 304 ( $< 0.05\%$  C, 18% Cr, 10% Ni) and 316Ti ( $< 0.06\%$  C, 17% Cr, 12% Ni, 2% Mo, 0.5% Ti), CoCr alloys Stellite 21 (28% Cr, 6% Mo) and L605 (20% Cr, 15% W, 10% Ni) for ion implantation as well as different Mg alloys for deposition experiments. All values are given in wt %.

The temperature was either adjusted by varying the pulse frequency, starting with a high repetition rate at room temperature and leveling off at a reduced value for the respective equilibrium temperature or by using additional IR lamps for a preheating before the start of the ion implantation. The temperatures varied between 250 and 750  $^{\circ}\text{C}$  with process times up to 3 hours, leading to total incident ion fluences up to  $5.0 \times 10^{18} \text{ cm}^{-2}$  [29].

For the coatings on Mg alloys, either ion beam sputtering (IBS) or vacuum arc deposition (VAD) was employed [26]. The ion beam sputtering experiments were performed in an UHV chamber using Argon ions from 800 to 1200 eV [30]. The angle between the ion source and the substrate normal was  $45^{\circ}$  with the target normal dividing this angle into two equal parts. The respective distances were 15 cm. Beside sputtered atoms with a kinetic energy between 1 and 5 eV, high energy backscattered Ar ions were impinging on the substrate during the film deposition, yielding an average ion energy of 8 – 15 eV per deposited particle. VAD was either used in conjunction with IBS or as a stand-alone process. At a total current of 100 A, an ion current of about 10 A could be extracted from the cathode. Using appropriate filtering techniques, macroparticles emitted from the cathode were suppressed at the expense of a reduced ion current. Average energies of 15 – 45 eV were typical for the stand-alone mode while values of 10 – 25 eV can be estimated for the combination with IBS, depending on the relative ion current densities.

The phase composition was studied by X-ray diffraction (XRD) in Bragg-Brentano geometry using  $\text{Cu K}\alpha$  radiation. The elemental concentration distributions were measured with elastic recoil detection analysis (ERDA) employing  $^{197}\text{Au}^{15+}$  ions at energies around 200 MeV. Additionally, secondary ion mass spectrometry (SIMS) was performed with a time-of-flight set-up with  $\text{Ga}^+$  as primary beam for analysis and  $\text{Cs}^+$  as secondary beam for depth profiling

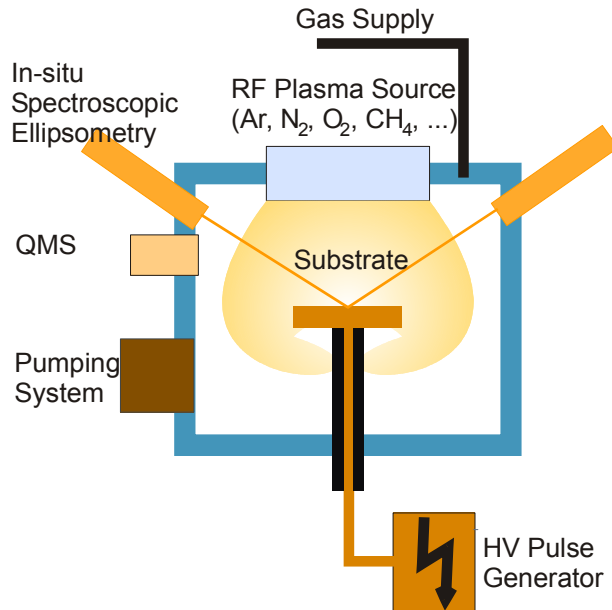


**Figure 2 - Experimental setup used for plasma immersion ion implantation. As the plasma surrounds the whole substrate, simultaneous and homogeneous implantation is achieved.**

### 3. RESULTS AND DISCUSSIONS

The tradition of modern metallic biomaterials starts in the 18<sup>th</sup> century where materials with an excellent biocompatibility but low strength (i.e. gold, silver and platinum) were used. In contrast, materials as brass, copper and iron with sufficient strength show an increased corrosion rate. Thus, before the invention of modern metallurgy in the first half of the 20<sup>th</sup> century, resulting in stainless steel, CoCr and Ti alloys, no widespread use of biomaterials was possible [31]. Lightweight magnesium alloys were used early on, focusing on temporary, resorbable implants [32]. Beside different costs, a different combination of elastic modulus, yield strength and fracture toughness is observed in these materials. Hence, depending on the initial properties, modifications in corrosion and wear properties, as well as topography, have to be applied to a different extent to obtain satisfactory results for each class of materials.

#### 3.1 TITANIUM ALLOYS

Titanium alloys are widely renowned for their excellent biocompatibility, caused by the formation of a native oxide layer within a very short timeframe, thus passivating any free

surface rather immediately [33]. However, very low tribological properties leading to high friction coefficients and wear rates are original causes of debris accumulation near implants and aseptic loosening of these implants at very high causality rates [34]. At the same time, elevated level of titanium ions may be found in selected organs [35].

Using nitrogen or oxygen PIII, thin modified surface layers between 50 and 500 nm are observed in the temperature range from 265 – 750 °C, with sufficient diffusion processes already observed around 400 – 500 °C [36,37]. For all low temperature implantations, sharp box-like edges of the oxygen, respective nitrogen, depth profiles were found coinciding with the calculated ion ranges. This indicates high fluences beyond sputter saturation without any additional diffusion of the implanted atoms. Diffusion of nitrogen in titanium at temperatures beyond 300 °C leads to the evolution of profiles which closely resemble complementary error functions obtained in standard diffusion theory. Oxygen in Ti and Ti6Al4V results in a mixture of both processes with titanium diffusing towards the surface and forming a closed titania layer while oxygen diffusing into the bulk leads to interstitial oxygen within the titanium matrix. Correspondingly, closed layer of  $\text{TiO}_2$  (rutile), respective TiN, followed by a diffusion layer with oxygen or nitrogen in solid solution have been observed.

As a result, the tribological surface properties have been improved significantly after PIII treatment. Using a rotating ball-on-disc test, no significant difference in the wear rate of untreated Ti and Ti6Al4V was found, while oxygen implantation results in a wear reduction of at least two orders of magnitude (see Fig. 3), nearly independent of the base material. In contrast, nitrogen ion implantation leads to smaller reductions of the specific wear at lower loads, while values similar to those for oxides were found at the highest contact pressure of 1.4 GPa [37].

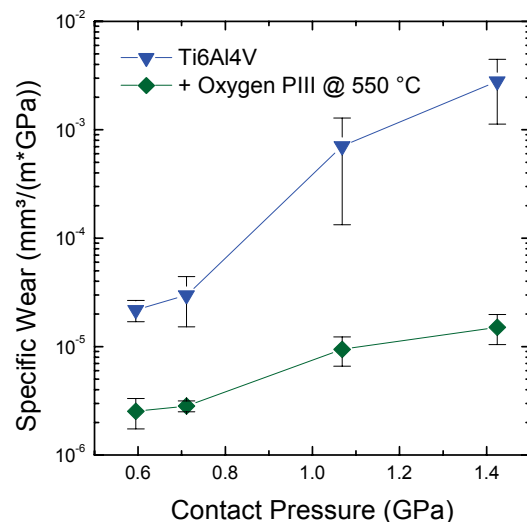


**Figure 3 - Specific wear fatigue time for oxygen implantation at different implantation temperatures during PIII and contact pressures during ball-on-disc wear test [37].**

There is a difference between PIII treatments and thermal oxidation of Ti alloys. A slower growth rate of the oxide in PIII is indicative of a supply limited process for PIII, leading to higher nucleation densities and smaller grains. At 550 °C, an average grain size of 75 nm is observed after PIII for Ti and Ti6Al4V, increasing to 150 nm at 700 °C [38,39]. In contrast, thermal oxidation at 700 °C shows crystallites of more than 300 nm in diameter [39]. Correspondingly, much higher wear rates are observed for thermally oxidized samples as these large grains are only insufficiently anchored in the substrate and after dislocating them, they act to increase third-party wear processes, as shown in Fig. 4. Beside uncontrolled annealing and diffusion processes in the base material, thermal oxidation at 900 °C leads to wear properties worse than those for the base material, despite a thick oxide layer.

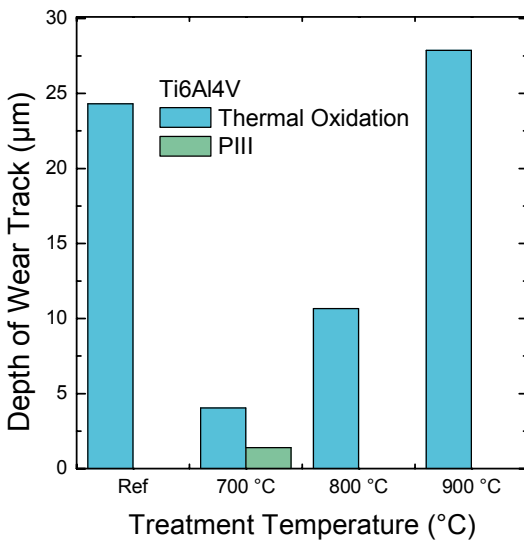


Figure 4 - Comparison of specific wear for PIII treated and thermally oxidized Ti6Al4V [39].

Subsequent animal tests after oxygen PIII using a rat model showed an improved osseointegration, as investigated by biomechanical pull-out tests as well as histological investigations and fluorescence microscopy [40]. No adverse toxicity of the implants, indicating no degraded corrosion resistance or repassivation behaviour was observed in these experiments. After oxygen PIII treatment, a much improved osseointegration was found for titanium, together with considerably higher pull-out forces [41].

It has to be mentioned that mechanical debris formation would have played only a minor role in these animal tests as no articulating surface was investigated. As a primary effect, a better osseointegration correlated with the nanotopography can be envisaged. For titanium alloys, the main effect for an enhanced biocompatibility rests within a modified surface topography and reduced wear rates by enhancing a native hard oxide layer

### 3.2 TiNi ALLOYS

NiTi is widely used as a biomaterial, however there are still no conclusive data on the biocompatibility of NiTi itself

with several studies showing that NiTi alloy is safe to use [42,43]. Thus, considerable effort has been employed to increase the thickness of the native oxide layer by ion implantation or by forming an additional nitride layer as surface barrier [44]. For oxygen PIII, again a surface layer consisting of pure TiO<sub>2</sub> (rutile) is formed at elevated temperatures, as can be seen from the depth profiles shown in Figs. 5 & 6 [45]. The composition itself cannot be inferred from the data, however independent information from Raman spectroscopy and resonant RBS measurements show that the composition of the sublayers correspond to the indicated structure of TiO<sub>2</sub>/Ni<sub>3</sub>Ti/NiTi.

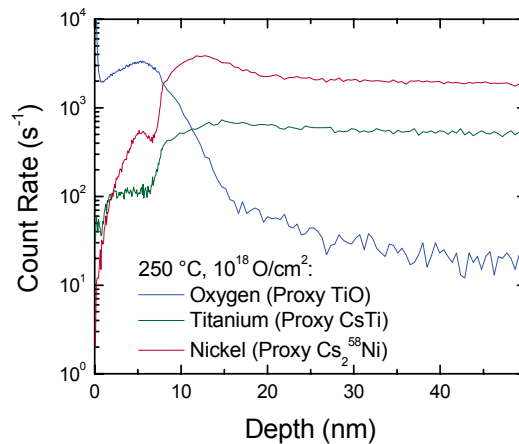


Figure 5 - SIMS profiles indicative of the layered structure formed after oxygen PIII at 250 °C. Following proxy ions were used: TiO (64 amu) for oxygen, CsTi (181 amu) for Ti and Cs<sub>2</sub>Ni (326 amu) for Ni [45].

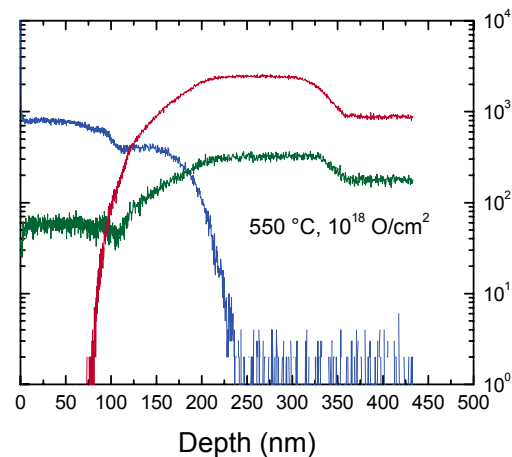


Figure 6 - SIMS profiles indicative of the layered structure formed after oxygen PIII at 550 °C [45].

Using the presented data, a comprehensive picture of the diffusion processes occurring at elevated temperatures during the implantation of oxygen into NiTi shape memory metal can be provided. Oxygen implantation leads to the formation of titania which is thermodynamically preferential to NiO. The growth of the oxide layer is a combination

of provision of additional oxygen from the surface and purging of Ni from this surface layer towards the underlying bulk with the chemical potential as the driving force. The titanium itself remains immobile during this process, as no change in the original Gaussian distribution of the Ti marker atoms in the oxide layer after oxygen implantation is observed. In addition, sputtering of the surface predominantly removes Ni [47]. However, this process itself is not sufficient to explain the Ni-free surface layer.

However, despite thicker oxide layer for higher PIII process temperatures, the fatigue time of oxygen implanted NiTi actually decreases with increasing implantation temperature. Nevertheless, higher fluences at the same temperature lead to an increase. Thus, a complex interplay of adhesion problems due to the sharp interface between the rutile surface and the NiTi intermetallic base material, coupled with complex diffusion phenomena can be proposed in this system [48]. The corrosion behavior can be improved quite straightforward, whereas the tribological properties depend very sensitively on the process parameters.

composition of the sublayers correspond to the indicated structure of  $\text{TiO}_2/\text{Ni}_3\text{Ti}/\text{NiTi}$  [46].

### 3.3 STAINLESS STEEL

Advances in the surface treatment of steels were continuously obtained in parallel with the development of new production technologies and alloys grades for steel. At the end of the 19<sup>th</sup> and in the early 20<sup>th</sup> century gas nitriding with reactive ammonia was introduced, followed by the use of inert nitrogen in plasma nitriding [49]. Nowadays, the standard parameters are in the temperature range around 500 to 650 °C and a treatment time of several hours, leading to a case depth of 100  $\mu\text{m}$  or more [50]. The obtained structure in the surface region consists of a double layer with a compound layer, a mixture of  $\epsilon\text{-Fe}_{2.3}\text{N}$  and  $\gamma'\text{-Fe}_4\text{N}$ , depending on the process parameters – followed by a diffusion layer.

However, stainless steels with a high chromium content – necessary for the formation of the protective  $\text{Cr}_2\text{O}_3$  surface layer – and corresponding low hardness and wear resistance values, necessitate low treatment temperatures around 350 – 400 °C to prevent the formation of chromium nitride precipitates, which completely compromise the corrosion resistance [51,52]. However, using energetic nitrogen ions in this temperature range, the formation of a very hard and wear resistant layer with an unusual high nitrogen content of up to 30 at.% in solid solution and a corresponding lattice expansion of some 5 – 15% is reported [53]. No nitride layer ( $\epsilon$  or  $\gamma'$ ) is accompanying this structure. This phase is generally called “expanded austenite” [54].

A diffusion limit growth is observed with the layer thickness approximately increasing with the square root of the process time. Here, the growth of the layer by diffusion processes is counteracted by a linear surface removal due to sputtering [55], which is more pronounced for LEI due to the higher current densities and lower ion energies compared to PIII at the same temperature. Fig. 7 shows respective results from time series at constant temperature for PIII and LEI, where the sputter yield for LEI is about 3.5 times higher than for

PIII, in rough accordance with estimates using TRIM [56]. At constant treatment time the layer thickness increases exponentially with higher temperatures, however with slightly lower diffusivities found for LEI, albeit showing no dependence on the steel grade. The activation energy for all processes is near constant around 0.6 – 1.0 eV, similar to literature values and representative for interstitial diffusion. The corrosion resistance is independent of the process, respective incident ion energy, however highly sensitive to temperature and ion energy [57]. Temperatures higher than 350 – 370 °C lead to an increased corrosion current while no CrN is visible in XRD data. At the same time, the corrosion potential of the untreated steel 316Ti seems to be an upper limit for all samples. For 316Ti the observed values are always close to the original value or more negative, while the values for 304 deviate from the base material (less corrosion resistant than 316Ti) in both directions.

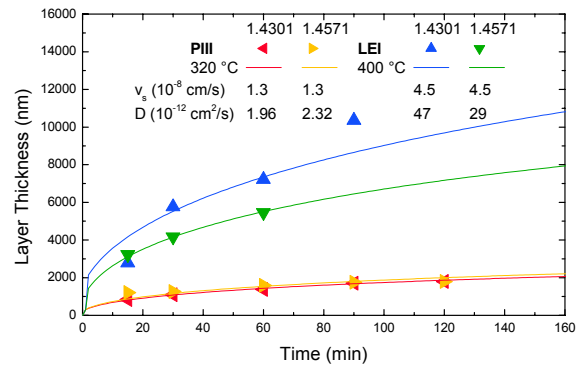


**Figure 7 - Evolution of layer thickness with time where surface sputtering and layer growth are competing processes for PIII and low energy broadbeam ion implantation (LEI) [54]. 1.4301 and 1.4571 correspond to 304 and 316Ti, respectively.**

In contrast, the mechanical properties are highly correlated with the layer thickness. Any influence of the process type, time and temperature is eliminated as the hardness and the corresponding wear resistance of the formed surface layer seems to be constant (see Fig. 8). However, the influence of the base material on the aggregate is still observed in the measured values, depending on the indentation depth and depth of the wear track. Details on these data can be found in previous works [58]. As a summary for austenitic stainless steels, an increase of the surface hardness by a factor of 4 up to 12 GPa and a decrease of the wear rate by 1 – 3 orders of magnitude is routinely obtained with a layer thickness exceeding 5  $\mu\text{m}$ . However, maintaining the excellent corrosion resistance requires a delicate processing window with upper limits on the temperature near 380 – 400 °C and corresponding short process times.

### 3.4 CrCo ALLOYS

CoCrMo alloys were used early for total-hip-replacements. However, the first generation of metal-on-metal THR was replaced by polyethylene bearings by the mid 70s as the pure metal implants showed high clinical failure rates. Due

to improved quality, a second generation with relatively low volumetric wear, compared to metal-polyethylene and ceramic polyethylene, is nowadays increasingly accepted. Despite lower wear debris release compared to alternative metal-PE designs, the number of emitted particles each year from a metal-on-metal articulating joint can still reach 1014 [59].

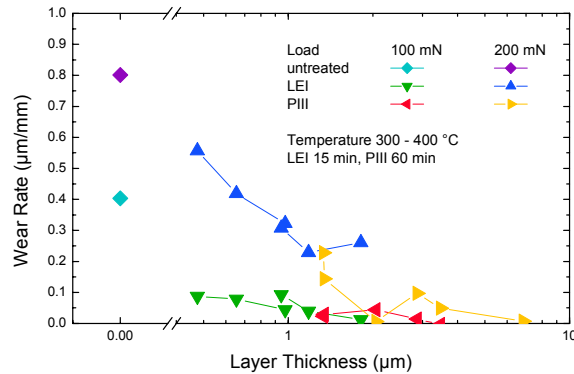


**Figure 8 - Wear rate measured in ball-on-disc configuration against layer thickness. For thinner layers, breakthrough does occur [54].**

Wrought and cast cobalt-base alloys (according ASTM F1537, respective DIN ISO 5832/12) are used for these implants and are considered to be biocompatible materials [60,61]. The biocompatibility of CoCrMo alloy is related closely to this material's excellent corrosion resistance, imparted by a thin passive oxide film that forms spontaneously on the alloy surface. X-ray photoelectron spectroscopy (XPS) analysis reveals that its composition is predominantly  $\text{Cr}_2\text{O}_3$  oxide with some minor contributions from Co and Mo oxides [62].

As only few publications show results on ion implantation of CoCr alloys, a large parameter space was investigated using PIII, including different CoCr alloys including L605, a biomedical CoCrNiW alloy (20 wt.% Cr, 10 wt.% Ni, 15 wt.% W, 3 wt.% Fe, 1.5 wt.% Mn., balance Co), SY21med (28 wt.% Cr, 5 wt.% Ni, balance Co), MP35N (20 wt.% Cr, 35 wt.% Ni, 10 wt.% Mo, 1 wt.% Fe, balance Co) and compared with Haynes 188 (22 wt.% Cr, 22 wt.% Ni, 14 wt.% W, 5 wt.% Fe, 1.25 wt.% Mn, 0.1 wt.% wt.% La, balance Co), an evolution with added La for high-temperature aerospace applications.

Fig. 9 compares the diffusion coefficients for PIII as calculated from the respective depth profiles for different process temperatures at a fixed process time of 60 minutes after reaching the process temperature and for different alloys. Comparing, the diffusion data of stainless steel and CoCr, a rather quite similar temperature dependence is observed, but with absolute values for stainless steel larger by a factor of about 10 than for CoCr. In both alloy classes two temperature regions with different activation energies can be distinguished: a low temperature area below 350 to about 400 °C with an energy EA of 1.0 – 1.1 eV and an high temperature area with lower values of 0.4 – 0.7 eV beyond the transition temperature.

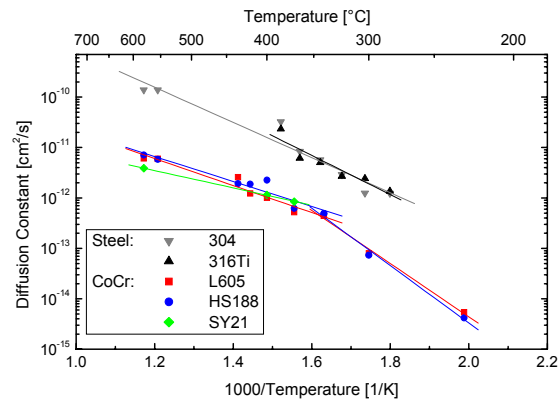


**Figure 9 - Arrhenius plot of resulting apparent diffusion coefficients as a function of temperature for the three investigated alloys after PIII. Additionally, data for stainless steel are included for comparison [63].**

The explanation of a phase transformation occurring at the transition point between the two activation energies is supported by XRD data showing that an expanded lattice is obtained below 400 °C, whereas CrN precipitates are formed above 400 °C [65]. This formation of CrN is identical in CoCr and austenitic stainless steel, with a slightly lower transition temperature observed for stainless steel than for CoCr alloys. The immobilisation of nitrogen atoms within CrN precipitates thus forms an alternative reaction channel, reducing the amount of nitrogen available for diffusion. As the formation of CrN is also a thermally activated process, a faster formation of CrN at higher temperatures implies the presence of a mobile nitrogen concentration decreasing with increasing temperature. The role of possible trapping mechanisms has to be investigated in further experiments but this is behind the scope of this paper. The CrN precipitates itself with a diameters of several nanometres [66] at a volume fraction of less than 25% should not lead to a significant blocking of the diffusion paths for nitrogen.

Similar to austenitic stainless steel, an increased surface hardness of up to 20 GPa and a reduced wear was observed. Using an alumina ball with a diameter of 4.76 mm as counterbody in ball-on-disc tests at a load of 1 N – resulting in a contact pressure of about 1 GPa – a qualitatively similar picture is emerging for all CoCr alloys [64]. A linear dependence of the wear volume on the wear path – or number of cycles – is observed for the untreated base material. However, the absolute values are again differing between  $0.35$  and  $3 \times 10^{-3} \mu\text{m}^3/\text{m}$  with SY21med showing the lowest value and HS188 the highest. Again, after PIII treatment the differences between the alloys nearly disappear with the absolute wear rates depending only on the PIII process temperature. The layer thickness itself is high enough to support the mechanical load without breakthrough during the experiment, except for HS188 implanted at 335 °C, where the wear behaviour of the non-implanted base material is observed at 4000 cycles and beyond. For MP35N and HS188, a decrease of the wear rate with increasing process temperature is observed, whereas a nearly inverse relation was

found for SY21med (shown in Fig. 10) with the lowest process temperature leading to the lowest wear rate among the implanted samples.

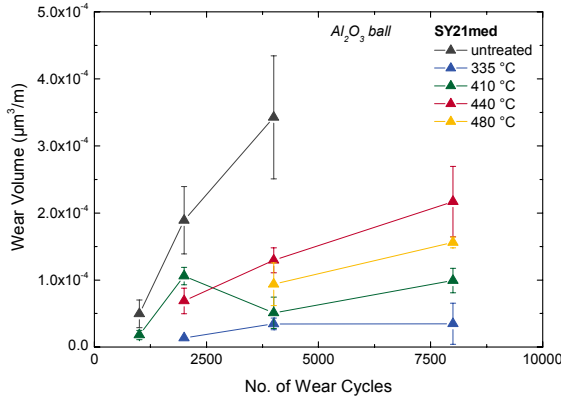


**Figure 10 - Wear volume as a function of wear cycles and PIII temperature. Please note the axis break [64].**

While the mechanical properties could be considerably improved, a strongly increased corrosion rate is observed after nitrogen insertion, starting already around 300 – 350 °C [67]. Thus, a careful balancing act between wear and corrosion has to be performed to find a compromise depending on the actual application. Alternatively, oxygen implantation results in very thin modified surface layers with a wear rate reduced by 50% and some progress on corrosion inhibition [68]. Furthermore, detailed investigations of additional influences of the topography are necessary

### 3.5 Mg ALLOYS

While the release of metallic ions from the previously discussed alloys varies between neutral and negative, the additional provision of  $Mg^{2+}$  ions can be classified as beneficial [69,70]. Furthermore, Mg is supposed to facilitate the osseointegration through its strong binding to phosphates. At the same time, the elastic modulus of pure Mg is much closer to that of bone than any other metallic biomaterial (including NiTi shape memory alloys). As a consequence, early uses in trauma surgery date back to the beginning of the 20<sup>th</sup> century [32,71]. However, unprotected magnesium alloys still show excessively large corrosion rates of 0.5 – 50 mm/year, which are still restricting their widespread use for biomedical applications [72,73] as the necessary bone regeneration rates is too slow to allow a replacement of any temporary resorbable implant within 6 – 8 weeks. A fast corrosion at the physiologically present pH of 7.4 – 7.6 and the high chlorine concentration are generally accompanied by hydrogen evolution, however it is reasonable to believe that this does not constitute a major problem [74,75].

Beside a reduction of detrimental elements like Fe, Ni and Cu [76] or addition of biotolerable elements, e.g. Zn, Mn, Ca and rare earth elements [73], the formation of a nanostructured or amorphous structure are also beneficial

for lower corrosion rates [77]. In this last group, nanostructured Mg-based coatings by PVD techniques have been investigated [26]. Besides a lower corrosion rate, these novel thin films are characterized by a rather homogeneous dissolution, thus avoiding the enrichment of more noble alloying elements and residual precipitates being converted in non-soluble particles. Both of these effects are highly detrimental for the use of Mg-alloys as resorbable biomaterials. In principle, this concept can be transferred to any available Mg alloy system.

Fig. 11 shows the measured corrosion rates in 0.5% NaCl solution for different PVD thin film alloys, compared with as-cast Mg. A reduction between a factor of 5 and 100 is observed, depending on the composition. For all alloys except  $MgAl_{20}Ti_{59}$ , a shift of the corrosion potential of the thin film by about – 200 to – 300 mV towards more negative values was observed [78], indicating the formation of a cathodic protection layer. At the same time, a much more homogeneous dissolution was found for the thin film coatings [79,80], compared to the as-cast alloys, which consist exclusively of the  $\alpha$ -phase with all alloying elements or impurities in solid solution. The formation of passive films is much easier on these coatings, visible in a reduced weight loss rate at longer immersion times (see Fig. 12). The incorporation of Al and/or Zn obviously stabilises the passive film based on  $Mg(OH)_2$  thus offering higher corrosion protection for the AZ91D coating compared to the pure Mg coating. Thus, a superior biocompatibility can be postulated for these PVD coatings as the most critical effects of as-cast alloys are avoided: A less pronounced release of potentially toxic Al and rare earth ions as well as the release of metallic particles which will be distributed throughout the whole body and be subjected to increased corrosion rates when liberated from the Mg matrix.

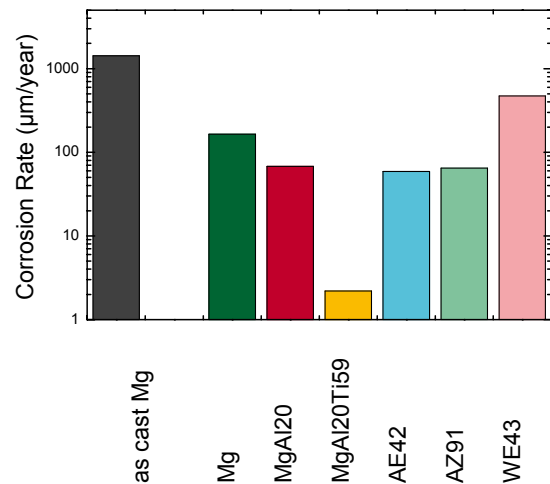


**Figure 11 - Corrosion rate for thin film coatings with different compositions. As-cast Mg is included for comparison [78].**

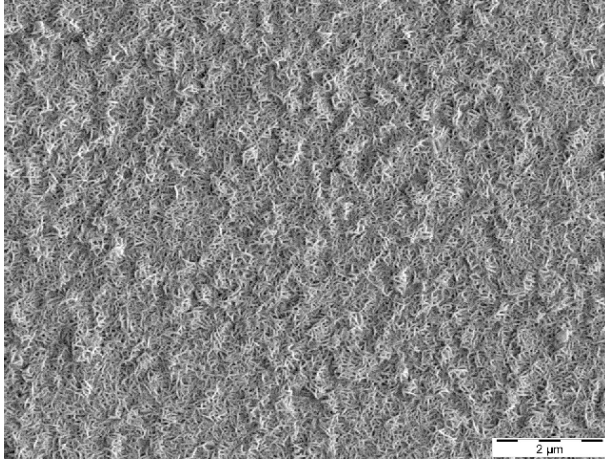


Figure 12 - Passive film formation on cp-Mg coatings [79].

#### 4. CONCLUSIONS

Using ion implantation as a physical surface modification method, it is possible to improve the biocompatibility and bioactivity of metals. Nevertheless, a complex relationship exists between implantation and biological response as several surface properties are modified simultaneously. Beside corrosion properties, surface topography, surface energy and tribological properties have to be mentioned. All major classes of metallic alloys employed as biomaterials have been successfully modified. For titanium alloys, the main point is an increased wear resistance in conjunction with a highly structured surface on the nano- and micro-scale, which can be simultaneously obtained by nitrogen or oxygen insertion. In contrast, an increased surface hardness and wear resistance was obtained for stainless steel and CoCr alloys after nitrogen implantation. However, process conditions require special attention for these materials as an increased surface corrosion and subsequent release of toxic elements is quite easily obtained. Similarly, biodegradable magnesium alloys with an increased corrosion resistance have been demonstrated, while the content of toxic elements or undesired insoluble particles has been reduced.

#### ACKNOWLEDGEMENTS

Darina Manova and Johanna Lutz are acknowledged for experimental work. Parts of this work were supported by European Regional Development Fund (ERDF) and the state of Saxony in project 12613/2085, as well as the German Federation of Industrial Research Associations (AIF) in project KF0189606FK7.

#### REFERENCES

1. MCKAY, D.S.; GIBSON, E.K.; THOMAS-KEPRTA, K.L.; VALI, H.; ROMANEK, C.S.; CLEMETT, S.J.; CHILLIER, X.D.F.; MAECHLING, C.R.; ZARE, R.N., *Science* 273 (1996) 924-930.

2. HAECKEL, E., *Kunstformen der Natur*, Bibliographisches Institut, Germany, 1899-1904.
3. THOMPSON, D.W., *On Growth and Form*, Cambridge University Press, USA, 1917.
4. KROTO, H.W., *Angewandte Chemie International Edition* 31 (1992) 111-129.
5. BALL, P., *Nature's Patterns*, Oxford University Press, Great Britain, 2009.
6. BAURSCHMIDT, P.; SCHALDACH, M., *Journal of Bioengineering* 1 (1977) 261-278.
7. SCHWARTZ, Z.; OLIVARES-NAVARRETE, R.; WIELAND, M.; COCHRAN, D.L.; BOYAN, B.D., *Biomaterials* 30 (2009) 3390-33966.
8. LANGER, R.; TIRRELL, D.A., *Nature* 428 (2004) 487-492.
9. HENCHAND, L.L.; POLAK, J.M., *Science* 295 (2002) 1014-1017.
10. BÖHLER, M.; KANZ, F.; SCHWARZ, B.; STEFFAN, I.; WALTER, A.; PLENK, H.; KNAHR, K., *Journal of Bone Joint Surgery - British Volume* 84B (2002) 128-136.
11. ELAGLI, K.; HILDEBRAND, H.J.; BREME, J., *International Biomaterials Symposium Transactions* 26 (1994) 262-263.
12. EL FENINAT, F.; LAROCHE, G.; FISET, M.; MANTOVANI, D., *Advanced Engineering Materials* 4 (2002) 91-104.
13. BÜSCHER, R.; TÄGER, G.; DUDZINSKI, W.; GLEISING, B.; WIMMER, M.A.; FISCHER, A., *Journal of Biomedical Materials Research B* 72 (2001) 206-214.
14. NEL, A.; XIA, T.; MÄDLER, L.; LI, N., *Science* 311 (2006), 622-627.
15. CURTIS, A.S.; WILKINSON, C.D., *Journal of Biomaterials Science Polymer Edition* 9 (1998) 1313-1329.
16. WOJCIAK-STOTHARD, B.; CURTIS, A.; MONAGHAN, W.; MACDONALD K.; WILKINSON, C., *Experimental Cell Research* 226 (1996) 426-435.
17. ELWING, H.; NILSSON, B.; SVENSSON, K.E.; ASKENDAHL, A.; NILSSON, U.R.; LUNDSTRÖM, I., *Journal of Colloid and Interface Science* 125 (1988) 139-145.
18. NASTASI, M.; MAYER, J.W., *Ion Implantation and Synthesis of Materials*, Springer, Germany, 2006, pp. 77-90.
19. BOXMAN, R.L.; MARTIN P.J.; SANDERS, D.M., *Handbook of Vacuum Arc Science and Technology*, Noyes Publications, USA, 1995.
20. ANDERS, A.; ANDERS, S.; BROWN, I.G.; DICKINSON M.R.; MACGILL, R.A., *Journal of the Vacuum Science and Technology B* 12 (1994) 815-820.
21. SCHNEIDER, J.M.; ROHDE, S.; SPROUL, W.D.; MATTHEWS, A., *Journal of Physics D* 33 (2000) R173-R186.
22. THORNTON, J.A., *Journal of Vacuum Science and Technology A* 4 (1974) 3059-3065.
23. OSTWALD, W., *Zeitschrift für Physikalische Chemie* 34 (1900) 495-503 (1900).
24. OHL, R.S., *Bell System Technology Journal* 31 (1952) 104-121.
25. CUOMO, J.J.; ROSSNAGEL, S.M.; KAUFMAN, H.R., *Handbook of Ion Beam Processing Technology*, Noyes Publications, USA, 1989.
26. BOHNE, Y.; MANOVA, D.; BLAWERT, C.; STÖRMER, M.; DIETZEL, W.; MÄNDL, S., *Nuclear Instruments Methods B* 257 (2007) 392-396.
27. CONRAD, J.R.; RADTKE, J.L.; DODD R.A.; WORZALA, F.J., *Journal of Applied Physics* 62 (1987) 4591-4596.
28. TENDYS, J.; DONNELLY, I.J.; KENNY, M.J.; POLLOCK, J.T.A., *Applied Physics Letters* 53 (1988) 2143-2145.
29. MÄNDL, S.; MANOVA, D.; RAUSCHENBACH, B., *Journal of Physics D: Applied Physics* 35 (2001) 1141-1148.

30. ZEUNER, M.; SCHOLZE, F.; NEUMANN, H.; CHASSÉ, T.; OTTO, G.; ROTH, D.; HELLMICH A.; OCKER, B., *Surface Coatings Technology* 142/144 (2001) 11-20.
31. WINTERMANTEL, E.; HA, S.-W., *Biokompatible Werkstoff und Bauweisen*, Springer, Germany, 2002, pp. 121-125.
32. LAMBOTTE, A., *Bulletins et Mémoires de la Société Nationale de Chirurgie* 28 (1932) 1325-1334.
33. GEETHA, M.; SINGH, A.K.; ASOKAMANI, R.; GOGIA, A.K., *Progress in Materials Science* 54 (2009) 397-425.
34. SIOSHANSI, P.; OLIVIER, R.W.; MATTHEWS, F.D., *Journal of Vacuum Science and Technology A* 3 (1985) 2670-2674.
35. SCHLIEPHAKE, H.; LEHMANN, H.; KUNZ, U.; SCHMELZEISEN, R., *International Journal of Oral and Maxillofacial Surgery* 22 (1993) 20-25.
36. LUTZ, T.; GERLACH, J.W.; MÄNDL, S., *Surface and Coatings Technology* 201 (2007) 6690-6694.
37. MÄNDL, S., *Surface and Coatings Technology* 201 (2007) 6833-6838.
38. MÄNDL, S.; THORWARTH, G.; SCHRECK, M.; STRITZKER, B.; RAUSCHENBACH, B., *Surface and Coatings Technology* 125 (2000) 84-88.
39. DIAZ, C.; LUTZ, J.; MÄNDL, S.; GARCÍA, J.A.; MARTÍNEZ, R.; RODRÍGUEZ, R.J.; DE DAMBORENEA, J.J.; ARENAS, M.A.; CONDE, A., *Physica Status Solidi c* 5 (2008) 947-951.
40. MÄNDL, S.; KRAUSE, D.; THORWARTH, G.; SADER, R.; ZEILHOFER, F.; HORCH, H.H.; RAUSCHENBACH, B., *Surface and Coatings Technology* 142/144 (2001) 1046-1050.
41. MÄNDL, S.; SADER, R.; KRAUSE, D.; THORWARTH, G.; ZEILHOFER, H.-F.H.; HORCH, H.; RAUSCHENBACH, B., *Biomolecular Engineering* 19 (2002) 129-132.
42. EL FENINAT, F.; LAROCHE, G.; FISET, M.; MANTOVANI, D., *Advanced Engineering Materials* 4 (2002) 91-104.
43. SHABALOVSKAYA, S.A., *Biomedical Materials Engineering* 12 (2002) 69-109.
44. YEUNG, K.W.K.; POON, R.W.Y.; CHU, P K.; CHUNG, C.Y.; LIU, X.Y.; LU, W.W.; CHAN, D.S.; CHAN, C.W.; LUK, K.D.K.; CHEUNG, K.M.C., *Journal of Biomedical Materials Research A* 82 (2005) 403-414.
45. LUTZ, J.; LINDNER J.K.N.; MÄNDL, S., *Applied Surface Science* 255 (2008) 1107-1109.
46. SCHIRMER, S.; LINDNER, J.K.N.; MÄNDL, S., *Nuclear Instruments Method B* 257 (2007) 714-717.
47. TAN, L.; CRONE, W.C., *Acta. Materialia* 50 (2002) 4449-4460.
48. MÄNDL, S.; FLEISCHER, A.; MANOVA, D.; RAUSCHENBACH, B., *Surface and Coatings Technology* 200 (2006) 6225-6229.
49. LIEDTKE, D., *Wärmebehandlung von Eisenwerkstoffen: Nitrieren und Nitrocarburieren*, Expert Verlag, Germany, 2006.
50. STAINES, A.M., *Heat Treatment of Metals* 4 (1990) 8592.
51. MENTHE, E.; RIE, K.-T., *Surface and Coatings Technology* 116/119 (1999) 199-204.
52. MCCAFFERTY, E., *Corrosion Science* 42 (2000) 1993-2011.
53. ICHII, K.; FUJIMARA, K.; TAKASE, T., *Technological Reports of Kansai University* 27 (1986) 135-144.
54. MÄNDL, S., *Plasma Processes and Polymers* 4 (2007) 239-245.
55. MÖLLER, W.; PARASCANDOLA, S.; TELBIZOVA, T.; GÜNZEL, R.; RICHTER, E., *Surface and Coatings Technology* 136 (2001) 73-79.
56. ZIEGLER, J.F.; BIRSACK, J.P.; LITTMARK, V., *The Stopping and Range of Ions in Solids*, Pergamon, USA, 1986.
57. MÄNDL, S.; MANOVA, D.; NEUMANN, H.; PHAM, M.T.; RICHTER, E.; RAUSCHENBACH, B., *Surface and Coatings Technology* 200 (2005) 104-108.
58. MANOVA, D.; MÄNDL, S.; NEUMAN, H.; RAUSCHENBACH, B., *Surface and Coatings Technology* 200 (2005), 137-140.
59. DOORN, P.F.; CAMPBELL, P.A.; WORRALL, J.; BENYA, P.D., MCKELLOP, H.A., *Journal of the Biomedical Materials Research* 42 (1998) 103-111.
60. LONG, M.; RACK, H.J., *Biomaterials* 19 (1988) 1621-1639.
61. KATTI, K.S., *Colloids Surfaces B - Biointerfaces* 39 (2004) 133-142.
62. MILOSEV, I.; STREHBLOW, H.H., *Electrochimica Acta* 48 (2003) 2767-2774.
63. LUTZ, J., LEHMANN, A.; MÄNDL, S., *Surface Coatings Technology* 202 (2008) 3747-3753.
64. LUTZ, J.; MÄNDL, S., *Plasma Processes and Polymers* 6 (2009) 565-569.
65. LUTZ, J.; GERLACH, J.W.; MÄNDL, S., *Physica Status Solidi a* 205 (2008) 980-984.
66. MANOVA, D.; HÖCHE, T.; HIRSCH, D.; MÄNDL, S.; NEUMANN, H., *Surface Coating Technology* 202 (2008) 2443-2447.
67. ÖZTÜRK, O.; TÜRKAN, U.; EROĞLU, A.E., *Surface Coatings Technology* 200 (2006) 5687-5697.
68. DIAZ, C.; LUTZ, J.; MÄNDL, S.; GARCÍA, J.A.; MARTÍNEZ, R.; RODRÍGUEZ, R.J., *Nuclear Instruments Method B* 267 (2009), 1630-1633.
69. SARIS, N.L.; MERVAALA, E.; KARPPANEN, H.; KHAWAJA, J.A.; LEWENSTAM, A., *Clinica Chimica Acta* 294 (2000) 1-26.
70. STANDING COMMITTEE ON THE SCIENTIFIC EVALUATION OF DIETARY REFERENCE INTAKES, FOOD AND NUTRITION BOARD, INSTITUTE OF MEDICINE, *Dietary Ref Intakes for Calcium Phosphorus Magn Vitamin D and Fluoride*, National Academy Press, USA, 1997, pp. 190-249.
71. STAIGER, M.P.; PIETAK, A.M.; HUADMAI, J.; DIAS, G., *Biomaterials* 27 (2006) 1728-1734.
72. KAINER, K.U., *Magnesium-Eigenschaften Anwendungen Potentiale*, VCH, Germany, 2000.
73. ZENG, R.; DIETZEL, W.; WITTE, F.; HORT, N.; BLAWERT, C., *Advanced Engineering Materials* 10 (2008) B3-B14.
74. WITTE, F.; REIFENRATH, J.; MUELLER, P.P.; CROSTACK, H.A.; NELLESEN, J.; BACH, F.W.; BORMANN, D.; RUDERT, M., *Materialwissenschaft und Werkstofftechnik* 37 (2006) 504-508.
75. WITTE, F.; KAESE, V.; HAFERKAMP, H.; SWITZER, E.; MEYER-LINDENBERG, A.; WIRTH, C.J.; WINDHAGEN, H., *Biomaterials* 26 (2005) 3557-3563.
76. SONG, G.; ATRENS, A., *Advanced Engineering Materials* 1 (1999) 11-33.
77. WANG, H.; ESTRIN, Y.; FU, H.; SONG, G.; ZÚBEROVÁ, Z., *Advanced Engineering Materials* 9 (2007) 967-972.
78. BOHNE, Y.; MANOVA, D.; BLAWERT, C.; STÖRMER, M.; DIETZEL, W.; MÄNDL, S., *Surface Engineering* 23 (2007) 339-343.
79. BLAWERT, C.; LUTZ, J.; PRAGER-DUSCHKE, A.; SCHARNAGL, N.; STÖRMER, M.; MANOVA, D.; MÄNDL, S., *Plasma Processes and Polymers* 6 (2009) 5690-5694.
80. BLAWERT, C.; HEITMANN, V.; DIETZEL, W.; STÖRMER, M.; BOHNE, Y.; MÄNDL, S.; RAUSCHENBACH, B., *Materials Science Forum* 539-543 (2007) 1679-1684.